Effect of Curvature, Contact Angle, and Interfacial Subcooling on Contact Line Spreading in a Microdrop in Dropwise Condensation

Ling Zheng, Ying-Xin Wang, Joel L. Plawsky, and Peter C. Wayner, Jr.*

The Isermann Department of Chemical Engineering, Rensselaer Polytechnic Institute, Troy, New York 12180-3590

Received January 11, 2002. In Final Form: April 17, 2002

The slow growth characteristics of a condensing ethanol sessile drop on a quartz substrate were studied experimentally. Using interference microscopy measurements of the transient liquid film profile (curvature) to obtain the pressure field and a Kelvin−Clapeyron model of interfacial mass flux to obtain the interfacial temperature difference, changes in the apparent contact angle were related to interfacial subcooling and, therefore, adsorption. We found that while the radius of curvature of the growing drop increased linearly with time, the apparent contact angle remained the same during slow growth at a constant condensation heat flux. The radii of curvature and the apparent contact angles at different axial locations were measured and compared. The results demonstrated that the curvature, the contact angle, the interfacial subcooling, the interfacial mass flux, the spreading velocity, and adsorption are coupled at the moving contact line. Motion and the apparent contact angle are governed by the condensed adsorbed thin film thickness and curvature at the contact line.

Introduction

Intermolecular interactions in the three-phase contact line region, where a liquid−vapor interface intersects a solid substrate, have been extensively studied because of their importance to many equilibrium and nonequilibrium phenomena such as contact angle, adsorption, spreading, evaporation, condensation, wetting, and stability. With regard to spreading, the relative importance of viscous stresses, slip, surface diffusion, molecular kinetics/dynamics, evaporation/condensation, excess free energy, contact angle, and film shape has not been resolved, experimentally or theoretically, at the contact line because of the molecular scale of the transport processes. Usually, spreading has been described using two types of isothermal nonvolatile liquid spreading models based on either molecular kinetics/dynamics and/or liquid-phase viscous flow (e.g., refs 1−27). However, since vapor-phase transport is also possible, a third type of isothermal model for contact line motion based on shape-induced condensation (Kelvin effect) was initially proposed by Wayner[28] and recently readdressed by Shanahan.[29] Briefly, a forced increase in the apparent contact angle (macroscopically measured) is associated with a change in the shape (thickness and curvature) and vapor pressure of the thin film in the immediate vicinity of the contact line. Condensation and motion result from this local change in vapor pressure and coupled increase in the apparent contact angle. This has also been extended to include the additional effect on spreading of an interfacial temperature jump on the vapor pressure (Clapeyron effect).[30] Since the chemical potential is a function of both temperature and pressure, we accept the premise that it is probably not possible to have spreading without phase change at the contact line. To address this premise, we present herein experimental results on contact line velocity in dropwise condensation and, thereby, show some of the characteristics of the coupling between condensation and contact line motion.

This Kelvin−Clapeyron model of spreading was suggested by the pioneering experimental results on the effect of vapor pressure on spreading by Hardy and Doubleday,[31] Bangham and Saweris,[32] and Bascom et al.[33] For the isothermal case, a seminal paper by Derjaguin et al.[34]

* Corresponding author. Tel: (518) 276-6199. Fax: (518) 276-4030. E-mail: wayner@rpi.edu.

(1) Blake, T. D.; Hayners, J. M. *J. Colloid Interface Sci.* **1969**, *30*, 421.
(2) Dussan, V. E. B.; Davis, S. H. *J. Fluid Mech.* **1974**, *65*, 71.
(3) Cherry, B. W.; Holmes, C. M. *J. Colloid Interface Sci.* **1969**, *29*, 174.
(4) Lopez, J.; Miller, C. A.; Ruckenstein, E. *J. Colloid Interface Sci.* **1976**, *56*, 460.
(5) Huh, C.; Scriven, L. E. *J. Colloid Interface Sci.* **1971**, *35*, 85.
(6) Hocking, L. M. *J. Fluid Mech.* **1977**, *79*, 209.
(7) Neogi, P.; Miller, C. A. *J. Colloid Interface Sci.* **1982**, *86*, 525.
(8) Hoffman, R. L. *J. Colloid Interface Sci.* **1983**, *94*, 470.
(9) Miller, C. A.; Ruckenstein, E. *J. Colloid Interface Sci.* **1974**, *48*, 368.
(10) Dussan, V. E. B. *Annu. Rev. Fluid Mech.* **1979**, *11*, 371.
(11) Starov, V. M. *Colloid J. USSR (Engl. Transl.)* **1983**, *45*, 1009.
(12) de Gennes, P. G. *Rev. Mod. Phys.* **1985**, *57*, 827.
(13) Cazabat, A. M. *Contemp. Phys.* **1987**, *28*, 347.
(14) Thompson, P. A.; Robbins, M. O. *Phys. Rev. Lett.* **1989**, *63*, 766.
(15) Koplik, J.; Banavar, J. R.; Willemsen, J. F. *Phys. Fluids A* **1989**, *1*, 781.
(16) Ehrhard, P.; Davis, S. H. *J. Fluid Mech.* **1991**, *229*, 365.
(17) Gribanova, E. V. *Adv. Colloid Interface Sci.* **1992**, *39*, 235.
(18) Hayes, R. A.; Ralston, J. *Langmuir* **1994**, *10*, 340.
(19) Chen, J. D.; Wada, N. *J. Colloid Interface Sci.* **1992**, *148*, 207.
(20) Koplik, J.; Banavar, J. R. *Annu. Rev. Fluid Mech.* **1995**, *27*, 257.
(21) Leger, L.; Joanny, J. F. *Rep. Prog. Phys.* **1992**, 431.
(22) Stoev, K.; Rame, E.; Ganoff, S. *Phys. Fluids* **1999**, *11*, 3209.
(23) Petrov, P. G.; Petrov, J. G. *Langmuir* **1995**, *11*, 3261.
(24) Schneemilch, M.; Hayes, R. A.; Petrov, J. G.; Ralston, J. *Langmuir* **1998**, *14*, 7047.
(25) Blake, T. D.; Clarke, A.; DeConinck, J.; deRuijter, M. J. *Langmuir* **1997**, *13*, 2164.
(26) Bankoff, S. G. *J. Heat Transfer* **1990**, *112*, 538.
(27) Pismen, L. M.; Rubinstein, B. Y. *Langmuir* **2001**, *17*, 5625.
(28) Wayner, P. C., Jr. *Langmuir* **1993**, *9*, 294.
(29) Shanahan, M. E. R. *Langmuir* **2001**, *17*, 3997.
(30) Wayner, P. C., Jr. *Colloids Surf., A* **1994**, *89*, 89.
(31) Hardy, W. B.; Doubleday, I. *Proc. R. Soc. Ser. A* **1922**, *200*, 550.
(32) Bangham, D. H.; Saweris, Z. *Trans. Faraday Soc.* **1938**, *34*, 554.
(33) Bascom, W. D.; Cottington, R. L.; Singleterry, C. R. In *Contact Angle, Wettability and Adhesion*; Gould, R. F., Ed.; Advances in Chemistry Series 43; American Chemical Society: Washington, DC, 1964; p 355.
(34) Derjaguin, B. V.; Nerpin, S. V.; Churaev, N. V. *Bull. Rilem* **1965**, *29*, 93.

10.1021/la020040b CCC: $22.00
Published on Web 06/01/2002

demonstrated the use of the disjoining pressure[35] gradient to evaluate the effect of surface film transfer on enhanced evaporation of liquid from capillaries. This led to the use of a Kelvin−Clapeyron model to describe the effects of both interfacial shape (capillary and disjoining pressure jumps) and interfacial temperature jump on the heat transfer characteristics of a stationary evaporating meniscus.[36] A more detailed analysis of the same configuration was done by Moosman and Homsy.[37] Additional research on the stationary evaporating extended meniscus has been done.[38−48] Lubrication theory has also been used to study the motion of volatile[26,49] and nonvolatile[16] drops subject to capillary, thermocapillary, and gravity forces. Using interfacial free energy and the Kelvin effect, Sharma[50] analyzed the effect of evaporation and condensation on thin film domains. The stability characteristics of thin film domains have also been addressed using the Kelvin−Clapeyron model.[26,50]

The main objectives of this paper are to (1) present unique experimental data on the slow growth characteristics of condensing ethanol sessile drops on quartz obtained using a constrained vapor bubble (CVB) heat transfer cell, (2) use a Kelvin−Clapeyron model and the Young−Dupre equation to determine the interfacial subcooling and the excess interfacial free energy, and (3) use these characteristics to discuss the spreading phenomena. We find that the CVB cell presented in Figures 1 and 2 is an effective experimental technique for enhancing our understanding of the effect of the chemical potential on motion in the contact line region. Briefly, the change in chemical potential per unit volume for a pure fluid in a gravitational field, $\Delta\mu$, is given by eq 1 in which the first group on the right-hand side comes from an isothermal change in the interfacial pressure jump (Kelvin effect) and the second group comes from an isobaric change in the interfacial temperature (Clapeyron effect).[45]

$$\Delta\mu = -(\Pi + \sigma_l K) + \frac{\rho_l \Delta h_m}{T_v}(T_{lv} - T_v) + \rho_l g\bar{x} \quad (1)$$

in which Π is the disjoining pressure, σ_l is the surface tension, K is the curvature, ρ_l is the liquid density, g is the acceleration constant, $\bar{x} = H - x$ is the local height in an extended meniscus, Δh_m is the heat of condensation, T_v is the reference vapor temperature, and T_{lv} is the temperature of the liquid−vapor interface. Since the gravitational term can be made small for the results reported below, it is included here for completeness.

Equation 1 can be used with kinetic theory to obtain eq 2 (Kelvin−Clapeyron model) for the net rate of interfacial condensation or evaporation, q''_{lv}:[5,51]

$$q''_{lv} = h_{lv}{}^{cl}(T_{lv} - T_v) - h_{lv}{}^{kl}(\Pi + \sigma_l K - \rho_l g\bar{x}) \quad (2)$$

where

$$h_{lv}{}^{cl} = \left(\frac{C^2 M}{2\pi R T_{lv}}\right)^{0.5} \frac{M P_v \Delta h_m{}^2}{R T_v T_{lv}}$$

$$h_{lv}{}^{kl} = \left(\frac{C^2 M}{2\pi R T_{lv}}\right)^{0.5} \frac{V_{lM} P_v \Delta h_m}{R T_{lv}}$$

where C is an accommodation coefficient, M is the molecular weight, R is the gas constant, and V_{lM} is the molar volume of the liquid. In general, eq 1 can be used to describe many equilibrium and nonequilibrium phenomena. For example, the first group on the right-hand side (rhs) can be used to obtain the equilibrium thickness profiles of an extended meniscus. For comparison, the variation of the curvature of the corner meniscus has been obtained experimentally as a function of height. Equating the first and second groups on the rhs gives the effect of superheat on the thickness of an adsorbed thin film at equilibrium[36,39] which is comparable to the Gibbs−Thompson equation used in crystal growth. In general, however, the coupling of the effects on the rhs of eq 1 easily leads to nonequilibrium systems that are unavoidable. The right-hand side of eq 2 is also a linearization of previously discussed exact results (e.g., refs 36, 37, 45, 47, 50, and 51). We find it convenient to use eq 2 to discuss our experimental results on dropwise condensation and contact line velocity.

The dropwise condensation process includes initial droplet formation, growth, removal, and renucleation on re-exposed sites. Previous studies on the microscopic mechanism of initial droplet formation presented experimental results to support one of two different hypotheses. One hypothesis assumes that droplets are generated and grow at nucleation sites, while portions of the surface between the growing droplets remain dry.[53,54] The second formation scenario is the film fracture hypothesis,[50,55] which was first proposed by Jakob.[55] The vapor condenses initially into an extremely thin liquid film on the solid surface, and droplets are formed by the rupture of the liquid film which eventually reaches a critical thickness estimated to be about 1 μm. This idea was later extended by Welch and Westwater[56] who observed dropwise condensation through a microscope using high-speed photography. They found that drops grow mainly by numerous coalescences. Condensation takes place mainly on the swept areas, and only slightly on the drops. A film forms on the swept area until a critical thickness of about 0.5 μm is reached at which time the film fractures to form new drops. Sugawara and Katusuta[57] utilized the excellent

(35) Derjaguin, B. V. *Colloid J. USSR (Engl. Transl.)* **1955**, *17*, 191.
(36) Potash, M., Jr.; Wayner, P. C., Jr. *Int. J. Heat Mass Transfer* **1972**, *15*, 1851.
(37) Moosman, S.; Homsy, G. M. *J. Colloid Interface Sci.* **1980**, *73*, 212.
(38) Kamotani, Y. *Proceedings of the Third International Heat Pipe Conference*, Palo Alto, CA; American Institute of Aeronautics and Astronautics: Reston, VA, 1978; p 128.
(39) Wayner, P. C., Jr.; Kao, Y. K.; LaCroix, L. V. *Int. J. Heat Mass Transfer* **1976**, *19*, 487.
(40) Renk, F.; Wayner, P. C., Jr.; Homsy, G. M. *J. Colloid Interface Sci.* **1978**, *67*, 408.
(41) Truong, J. G.; Wayner, P. C., Jr. *J. Chem. Phys.* **1987**, *87*, 4180.
(42) Mirzamoghadam, A. V.; Catton, I. *J. Heat Transfer* **1988**, *110*, 208.
(43) Holm, F. W.; Goplen, S. P. *J. Heat Transfer* **1979**, *101*, 543.
(44) Hallinan, K. P.; Chebaro, H. C.; Kim, S. J.; Chang, W. S. *J. Thermophys. Heat Transfer* **1994**, *8*, 709.
(45) Wayner, P. C., Jr. *Colloids Surf.* **1991**, *52*, 71.
(46) Stephan, P.; Busse, C. A. *Int. J. Heat Mass Transfer* **1992**, *35*, 383.
(47) Swanson, L. W.; Peterson, G. P. *J. Heat Transfer* **1995**, *115*, 195.
(48) Morris, S. J. S. *J. Fluid Mech.* **2001**, *432*, 1.
(49) Anderson, D. M.; Davis, S. H. *Phys. Fluids* **1995**, *7*, 248.
(50) Sharma, A. *Langmuir* **1998**, *14*, 4915.
(51) Padmakar, A. S.; Kargupta, K.; Sharma, A. *J. Chem. Phys.* **1999**, *110*, 1735.
(52) Wang, Y.-X.; Plawsky, J.; Wayner, P. C., Jr. *Microscale Thermophys. Eng.* **2001**, *5*, 55.
(53) McCormick, J. L.; Baer, E. *J. Colloid Sci.* **1963**, *18*, 208.
(54) Umur, A.; Griffith, P. *J. Heat Transfer* **1965**, *87*, 275.
(55) Jakob, M. *Mechanical Eng.* **1936**, *58*, 729.
(56) Welch, J. F.; Westwater, J. W. *Proceedings of the International Heat Transfer Conference*; American Society of Mechanical Engineers: New York, 1961; Part II, p 302.
(57) Sugawara, S.; Katusuta, K. *Proceedings of the Third International Heat Transfer Conference*, Chicago, IL; Science Press: Ephrato, PA, 1966; Vol. 2, p 354.

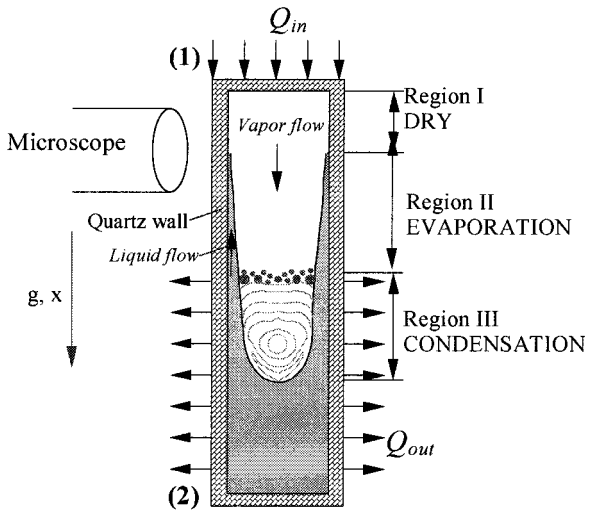

Figure 1. A schematic drawing of the vertical CVB in the earth's gravitational field. The liquid profile is for the front inside surface. At equilibrium, the liquid meniscus can wick to the top of the cell in the corner. The thermocouples on the quartz wall are not shown.

durability of poly(dimethylsiloxane) as a promoter to the copper cooling surface to observe condensation microscopically. Chen and Wada[19] studied the isothermal spreading dynamics of a drop edge using a laser light interference microscopy method. Lai[58] investigated theoretically the growth of a single spherical droplet due to condensation. Tanasawa[59] has written an excellent review on condensation. Herein, we use a set of equations presented by Sharma to study the apparent contact angle as a function of the excess free energy per unit area.[60] The reverse process of droplet evaporation has also been studied.[61,62]

In our partially wetting ethanol/quartz system, we observed qualitatively a very thin film of condensate in the area between the drops and the spots from which the drops departed. Although we could see some qualitative variation in the reflectivity between the droplets in the experiments discussed herein, these reflectivity changes indicated the presence of extremely thin films (much thinner than the 0.5 μm cited above and closer to a few nanometers). We find that the analysis of the presented nonequilibrium data using both the pressure and temperature fields gives unique insights into the physical phenomena present at the phase junction. Briefly, a temperature gradient across a glass cuvette (see Figure 1) partially filled with liquid gives well-controlled local regions of measurable rates of evaporation and condensation which can be modeled using interfacial concepts. We find that near the junction between the regions of evaporation and condensation, small rates of condensation can be easily viewed, recorded, and evaluated. Using interference microscopy measurements of the transient liquid film profile to obtain the pressure field and a Kelvin−Clapeyron model of interfacial mass flux to obtain the interfacial temperature difference, changes in the apparent contact angle are related to interfacial subcooling and, therefore, adsorption. We emphasize that we discuss measurements in only a small region of the cell under near-equilibrium local conditions, which occurs at the junction of the regions of condensation and evaporation.

Experimental Setup and Observations

Figure 1 shows a schematic drawing of the CVB cell designed to study the growth characteristics of an ethanol sessile droplet in a very small subregion of the cell. Briefly, the CVB was formed by underfilling with liquid an evacuated closed fused quartz cell, which had been heated to a high temperature during fabrication. The high temperature removal of surface hydroxyl groups gave a partially wetting system.[63] At isothermal equilibrium, the cell has been used to measure the Hamaker constant and disjoining pressure.[64] The quartz cell had a square cross section with sharp internal corners and internal dimensions of 3 × 3 × 40 mm. A thermoelectric heater was located on the top, and coolers on each side of the cell were located at 20 mm from the top. Besides the coolers, the CVB loses energy along its entire length by convection and radiation. Details regarding the experimental setup can be found from Wang et al.[52,65,66,67] For an isothermal completely wetting system, the liquid will coat all the walls of the chamber. On the other hand, for a finite contact angle system, some of the walls will have only an extremely small amount of adsorbed vapor which changes the surface properties of the solid−vapor interface. Liquid will fill at least a portion of the corners in both cases. If temperature $T_1 > T_2$ because of an external heat source in the evaporator, Q_{in}, and heat sink in the condenser, Q_{out}, energy flows from end 1 to end 2 by conduction in the walls and by an evaporation, vapor flow, and condensation mechanism. The condensate flows from end 2 toward end 1 because of the intermolecular force field which is a function of the film profile. The film profile, which gives the pressure jump at the liquid−vapor interface, is a function of the local thermal conditions on the surface. Due to the surface heat flux, there were temperature gradients in the cell with local regions of condensation, evaporation, and dryness. Both fluid flow and phase change were due to the interfacial temperature jump and the shape-dependent stress field (pressure) in the liquid resulting from the imposed external temperature field. The liquid thickness profile and contact angle were obtained using image-analyzing interferometry, in which naturally occurring interference fringes resulting from the reflection of monochromatic light at both the liquid−vapor and liquid−solid interfaces were recorded using a video camera attached to a microscope.[64] As presented in Figure 1, we observed three regions: region I (the dry region), region II (the evaporator region), and region III (the condenser region). In particular, the region of dropwise condensation was viewed through a microscope with a 50× objective and captured using a video camera, as shown in Figure 2. Monochromatic light (λ = 543.5 nm) from a Hg arc is used to illuminate the cell through the objective of the microscope. With a 50× objective, each of the 640 × 480 pixels measures the average reflectivity (thickness) of a region with a diameter of 0.1777 μm. The recorded images were then analyzed using image processing. The resulting liquid thickness profile gives the curvature and apparent contact angle.[52,64]

In region III, the wall temperature is lower than the vapor temperature. The vapor condensed into small discrete liquid drops which then grew and coalesced into larger drops, which were then absorbed into the bulk liquid in the corner. Closer to the cooler, the condensate formed a continuous, thicker liquid film on the flat surface of the glass. The condensation process is observable because of the presence of the naturally occurring interference. Wang et al.[52] studied the departure of a single condensed drop into a concave liquid film due to the intermolecular force gradient in region III. Herein, we discuss the growth characteristics of an ethanol droplet in region III before its symmetric profile is affected by the corner meniscus.

(58) Lai, C.-L. *J. Heat Transfer* **1999**, *121*, 632.
(59) Tanasawa, I. *Proceedings of the 10th International Heat Transfer Conference*, Brighton, U.K., 1994; Institution of Chemical Engineers: Rugby, Warwickshire, U.K.; Vol. 1, p 297.
(60) Sharma, A. *Langmuir* **1993**, *9*, 3580.
(61) Bindi, K. S.; Vu, D. T. *J. Phys. Chem.* **1989**, *93*, 3702.
(62) Rowan, S. M.; Newton, M. I.; McHale, G. *J. Phys. Chem.* **1995**, *99*, 13268.
(63) Hautman, J.; Klein, M. L. *Phys. Rev. Lett.* **1991**, *67*, 1763.
(64) DasGupta, S.; Plawsky, J. L.; Wayner, P. C., Jr. *AIChE J.* **1995**, *41*, 2140.
(65) Wang, Y.-X.; Plawsky, J.; Wayner, P. C., Jr. 34th National Heat Transfer Conference, Pittsburgh, PA, Aug 2000; paper NHTC2000-12201.
(66) Wang, Y.-X.; Zheng, L.; Plawsky, J.; Wayner, P. C., Jr. *J. Heat Transfer* **2002**, *124*, 1.
(67) Wang, Y.-X. A Study of The Vertical Constrained Vapor Bubble. Ph.D. Thesis, Rensselaer Polytechnic Institute, Troy, NY, 2001.

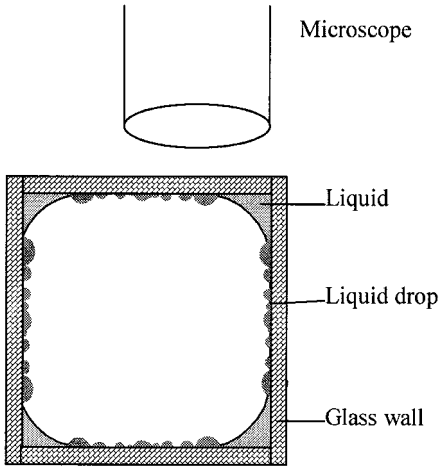

Figure 2. Dropwise condensation in region III.

Figures 3 and 4 illustrate the growth of a drop indicated by the arrow at axial locations $x = 3$ mm and $x = 4$ mm from the top, respectively. Since the heater is placed on the top of the CVB and the cooler is located at 20 mm from the top, there is a temperature distribution along the axial direction, which can be easily controlled. At $x = 4$ mm, the drop is closer to the cooler, and the temperature difference for the dropwise condensation between vapor and quartz wall (ΔT_{vw}) is larger. As the drop grows, the number of fringes increases and the fringe in the center alternates between dark and bright. The growth of the drop is caused by measurable direct condensation of vapor onto the small drop and possible condensation between the drops. Obviously, the spacing between fringes in Figure 4 is larger than that in Figure 3. In Figure 4, the fringe in the center alternates faster than that in Figure 3. An image-analyzing technique was developed to obtain curvature and apparent contact angle of the drop simultaneously.

Image Analysis for the Liquid Drop

In general, our image analysis technique was developed to analyze either a corner meniscus or a drop on a flat surface. Figure 5 represents both a meniscus in one of the corners of the cell with a general vertex angle of α ($Y-Z$ coordinate) and a drop on the flat surface of the cell ($Y'-Z'$ coordinate). As presented, the drop is not affected by the corner. Since our image analysis system was initially based on the concave liquid meniscus in the corner, a coordinate transformation is employed to analyze the experimental data for the convex drop.

First, for a meniscus, the corner is partially filled with the liquid, and the liquid forms an apparent finite contact angle of θ_c on the interior wall of the container. The coordinate axes are labeled on the figure. The Z-axis represents the thickness of the liquid film (δ). The Y-axis, which corresponds to one side of the container wall, represents the location of the film thickness profile. The vapor−liquid interface is assumed to be a part of a circle, and the center of the circle is located at point O. The local validity of this assumption was demonstrated by the final fit of the model to experimental data.[52,66] The coordinates of point O ($r \cos \theta_c$, $c + r \sin \theta_c$) are easily derived from geometric relations, where

$$c = r\frac{\sin\frac{\phi}{2}}{\sin\frac{\alpha}{2}}, \qquad \phi = \pi - (2\theta_c + \alpha)$$

The shape of a concave vapor−liquid interface at the corner of a container can thus be expressed as

$$(\delta - r \cos \theta_c)^2 + (y - c - r \sin \theta_c)^2 = r^2 \qquad (3)$$

Rearranging eq 3 while using the negative square root yields

$$y = c + r \sin \theta_c - \sqrt{r^2 - (\delta - r \cos \theta_c)^2} \qquad (4)$$

In our particular case of a square cross section, $\alpha = \pi/2$. Equation 4 describes the shape of the concave liquid film in the corner of a container using a YZ-coordinate system.

Since a liquid drop forms a convex vapor−liquid interface on the flat surface, the curvature of the liquid

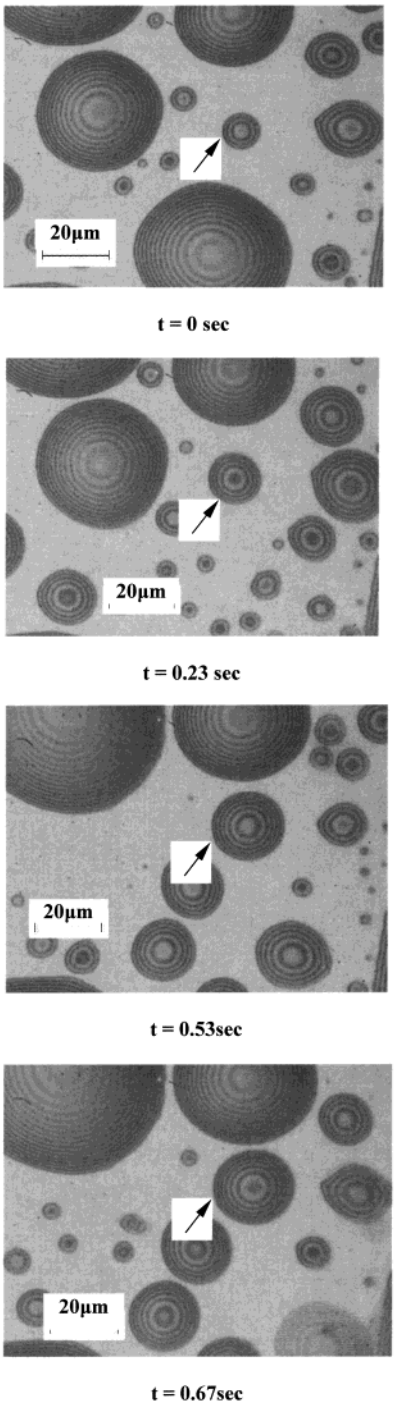

Figure 3. Drop profiles at different relative times at $x = 3$ mm.

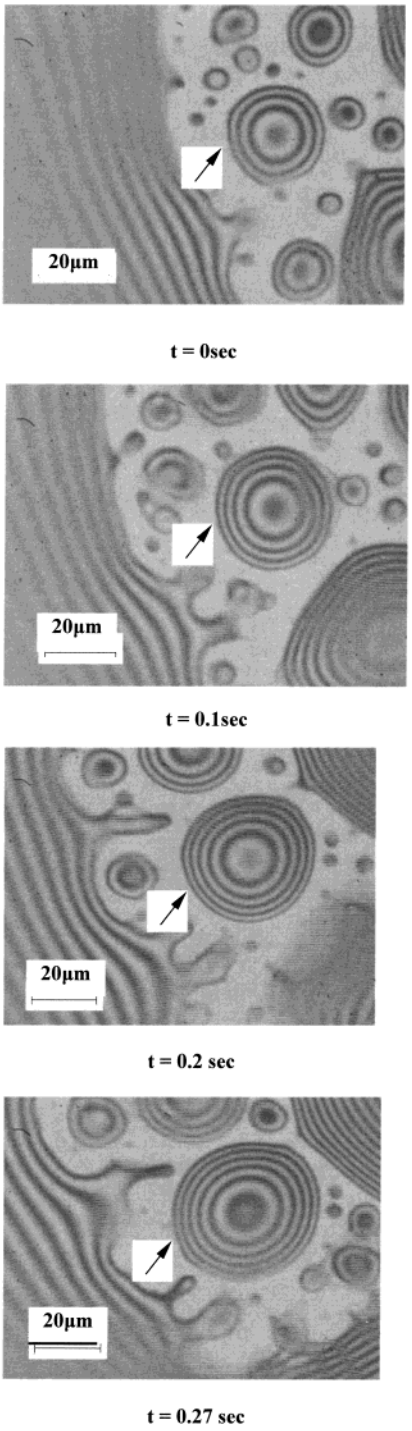

Figure 4. Drop profiles at different relative times at $x = 4$ mm.

drop on the flat surface cannot be obtained by directly applying the above equations. Experimentally, we can obtain the film thickness profile (δ'_{exp}) of the midplane of the drop. Therefore, for a midplane through the drop, we introduce a $Y'Z'$-coordinate system for a single radius of curvature shown in Figure 5 with the origin at point O″ and with the Y'-axis directed along the flat surface line O″B. The $Y'Z'$-system is devised so that theoretical film thickness profiles can be compared with experimental data. The Z'-axis represents the film thickness (δ') of the drop, and the Y'-axis represents the location (y') of the film thickness. To obtain the curvature of the drop by applying eq 4, we need to determine the transformation between the YZ-system and the $Y'Z'$-system. By geometrical derivations, the points in the YZ-system can be expressed in the $Y'Z'$-system by the following coordinate transformation:

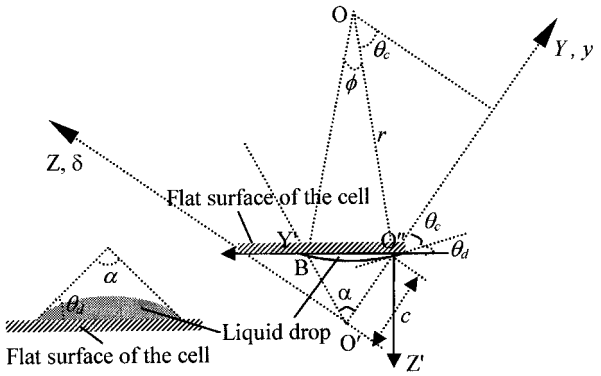

Figure 5. Coordinate transformation for the drop on the flat surface.

$$y = c - \frac{y' + \delta'}{\sqrt{2}} \tag{5a}$$

$$\delta = \frac{y' - \delta'}{\sqrt{2}} \tag{5b}$$

where δ and y denote the film thickness and the location of the film thickness in the YZ-system, respectively. δ' and y' denote the film thickness and the location in the $Y'Z'$-system. Substituting eqs 5a and 5b into eq 4 and rearranging gives

$$y' = -\frac{1}{2}\{\sqrt{2}r(-\cos\theta_c + \sin\theta_c) + \sqrt{2r^2(-\cos\theta_c + \sin\theta_c)^2 - 4[(\delta')^2 + \sqrt{2}r\delta'(\cos\theta_c + \sin\theta_c)]}\} \tag{6}$$

Using eq 6, the two unknowns, r and θ_c, can be obtained simultaneously by best-fitting the experimental film thickness profile of the drop. The apparent contact angle of the drop is then given by $\theta_d = (\pi/4) - \theta_c$, the radius of the curvature is $r_d = r$, and the curvature is $K_d = -2/r$ ($K_d < 0$ for the convex drop).

Theoretical Analysis

The dropwise condensation process includes initial droplet formation, growth, removal, and renucleation on re-exposed sites. Our paper discusses mainly the growth of the drop. The interfacial pressure difference at x is obtained using the augmented Young−Laplace equation:

$$P_v - P_l = \sigma_l K + \Pi \tag{7}$$

The disjoining pressure is neglected in the initial (experimental) portion of this paper since the film thickness is measured where $\delta > 0.1$ μm. The pressure level in the vapor, which is approximately uniform because of minimum resistance to vapor flow, is measured using a pressure transducer. The temperature of the vapor, T_v, in the region of condensation can be obtained from thermodynamic tables of $T_v(P_v)$.[68] Although the liquid−vapor interfacial temperature difference, $T_{lv} - T_v$, is too small to measure, it can be obtained using interference microscopy measurements of the transient liquid film profile to

(68) Vargaftik, N. B. *Tables on the Thermophysical Properties of Liquids and Gases*, 2nd ed.; Hemisphere Publishing: Washington, 1975; Chapter 4.

obtain the pressure field and a Kelvin−Clapeyron model of interfacial mass flux.

For a mass balance during condensation, the drop can be assumed to be a spherical cap since the liquid volume deviation near the contact line is very small. The volume of the drop can be obtained by measuring the radius of curvature and the apparent contact angle of the drop:

$$V = \frac{1}{3}\pi {r_d}^3(1 - \cos\theta_d)^2(2 + \cos\theta_d) \quad (8)$$

When the small effect of condensation in the ultrathin film region is neglected, a heat balance over the drop gives

$$\frac{d(\Delta h_m \rho_l V)}{dt} = -q''_{lv} A \quad (9)$$

where Δh_m is the latent heat of vaporization, A is the liquid−vapor interfacial area of the drop, $A = 2\pi {r_d}^2(1 - \cos\theta_d)$, and q''_{lv} is the heat flux for the drop. Assuming no horizontal flow in the peripheral ultrathin film region because of large viscous forces, the neglected volume would be, at most, only that associated with a thickness of a few nanometers. The sign of q''_{lv} is negative representing condensation.

On the basis of our experimental data presented below, we found that the apparent contact angle of the drop is almost constant for our conditions. Therefore, the heat flux is rewritten as

$$q''_{lv} = -\frac{\Delta h_m \rho_l (1 - \cos\theta_d)(2 + \cos\theta_d)}{2}\frac{dr_d}{dt} \quad (10)$$

Experimental data show that the radius of curvature for the growing drop increases linearly with time. Therefore, eq 10 can be combined with a Kelvin−Clapeyron model of interfacial mass flux to obtain the interfacial temperature difference. Using eq 1, eq 11 was obtained for the vapor pressure difference at the liquid−vapor interface at $\bar{x}$ for the nonisothermal case.[45]

$$P_{lv} - P_{vx} = \frac{V_l P_v}{R T_v}\left(-\Pi - \sigma_{lv}K + \rho_l g\bar{x} + \frac{\rho_l \Delta h_m \Delta T_{lvv}}{T_{lv}}\right) \quad (11)$$

where P_{lv} is the vapor pressure of the film at the liquid−vapor interface and P_{vx} is the bulk vapor pressure in the vapor cavity at the same height, $\bar{x}$. The interfacial temperature jump is $\Delta T_{lvv} = T_{lv} - T_v$, in which T_{lv} is the temperature at the liquid−vapor interface. T_v and P_v are the reference temperature and pressure at $\bar{x} = 0$ where $(\Pi + \sigma_{lv}K) = 0$, $\Pi > 0$ is the disjoining pressure or the excess free energy per unit volume of a completely wetting flat film, and $\sigma_l K > 0$ is the capillary pressure or the excess free energy per unit volume of a concave surface due to curvature. Herein, we use the same equation for the experimentally studied partially wetting CVB system where $\sigma_l K < 0$. We find that condensation occurs when $P_{lv} < P_{vx}$,

$$\frac{\rho_l \Delta h_m \Delta T_{lvv}}{T_{lv}} < (\Pi + \sigma_l K - \rho_l g\bar{x}) \quad (12)$$

For a partially wetting system, $\Pi < 0$ and $\Pi \Rightarrow 0$ as $\delta \Rightarrow \infty$. For a sessile drop, $K < 0$ and $K \Rightarrow 0$ as the drop grows. To obtain condensation with a bulk liquid and with an external heat loss to the surroundings, $\Delta T_{lvv} < 0$. As the absolute value of $\sigma_l K$ increases, more subcooling is needed.

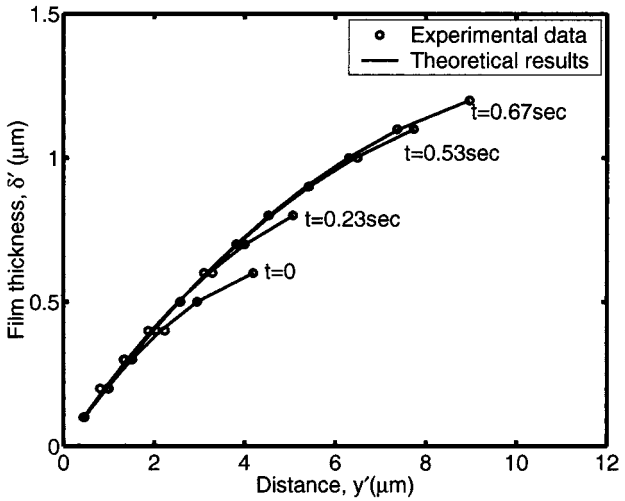

Figure 6. Film thickness profiles of the growing drop at $x = 3$ mm.

The use of eq 12 for the continuous corner meniscus connected to the pool is straightforward. However, the effect of $\rho g\bar{x}$ on the drop is not because it depends on a path in the ultrathin adsorbed film. Experimentally, we find that the quartz surface just below the region of dropwise condensation is covered by a relatively thick, flat film (Π, $K \approx 0$) of slowly draining condensate. Therefore, using this relatively thick, flat film as the reference for quasi-equilibrium, $\rho g\bar{x} \approx 0$. The use of this boundary condition does not affect the final conclusions.

Combining eqs 2 and 10 for the region where $\Pi = 0$, we obtain eq 13 for the interfacial temperature difference, which is a function of time,

$$\Delta T_{lvv} = \frac{1}{{h_{lv}}^{cl}}\left[-\frac{h_{fg}\rho_l(1 - \cos\theta_d)(2 + \cos\theta_d)}{2}\frac{dr_d}{dt} - {h_{lv}}^{kl}\frac{2\sigma_l}{r_d}\right] \quad (13)$$

The interfacial temperature difference can thus be obtained experimentally by measuring apparent contact angle, radius of curvature, and dr_d/dt.

Results and Discussions

Figures 3 and 4 show the growing drops with obvious differences at different axial locations. At the outset, we note that we are comparing our best data from two separate experiments which were taken at different vapor pressure levels: $P_v = 2.68 \times 10^4$ Pa and $T_v = 47$ °C at $x = 3$ mm; $P_v = 7.85 \times 10^4$ Pa and $T_v = 73$ °C at $x = 4$ mm. At $x = 4$ mm in Figure 4, the drop is closer to the location of the cooler, the temperature difference for the dropwise condensation between vapor and quartz wall (ΔT_{vw}) is larger, and the condensing mass flux is larger relative to $x = 3$ mm. The image-analyzing technique was used to obtain variations of the curvatures and apparent contact angles of the growing drop with time. The film thickness profiles corresponding to Figures 3 and 4 are presented in Figures 6 and 7, respectively. The circles represent experimental data, and the lines represent theoretical curve fitting results obtained from eq 6. For comparison, the locations of the first fringe at different times were plotted at the same location. The average film thickness of the drops increases as time increases.

Figure 8 shows a comparison of the variation of the radius of curvature with time at different locations. For

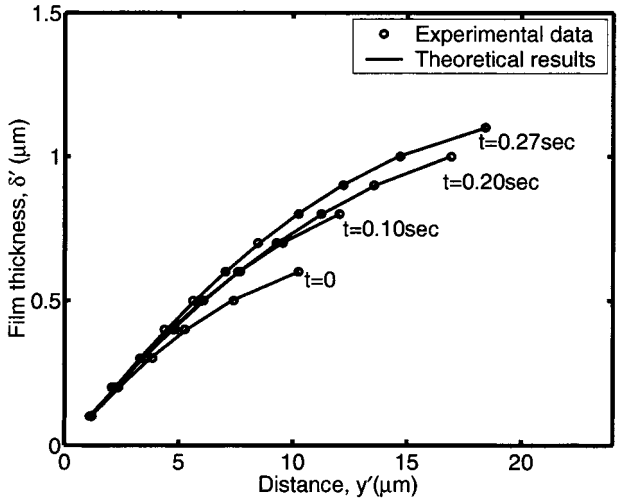

Figure 7. Film thickness profiles of the growing drop at $x =$ 4 mm.

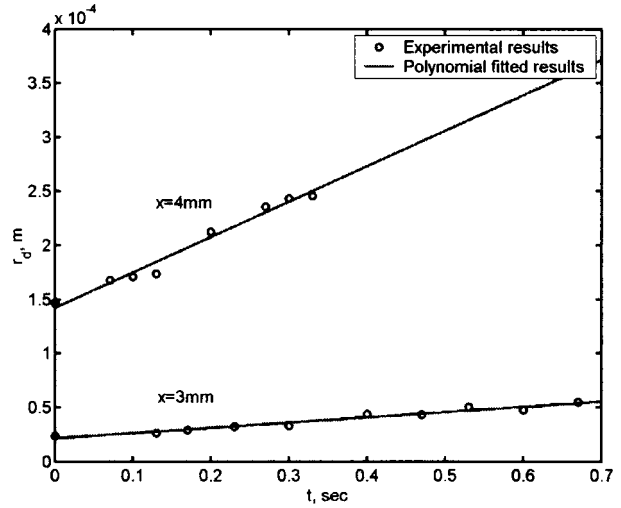

Figure 8. Comparison of radii of curvature for the growing drop at different locations.

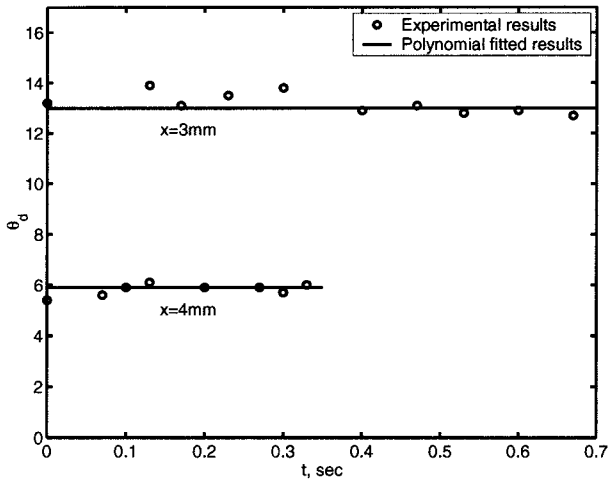

Figure 9. Comparison of apparent contact angles for the growing drop at different locations.

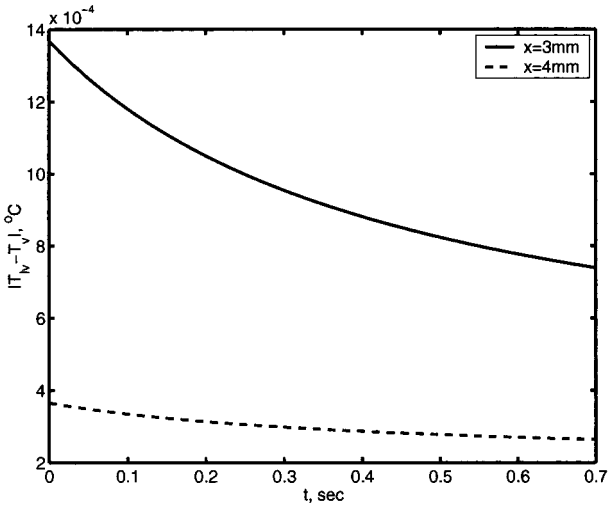

Figure 10. Comparison of the absolute value of the interfacial temperature difference, $|\Delta T_{lvv}|$, for the growing drop at different locations.

the drops at $x = 3$ mm, the radius of curvature of the growing drop increases linearly from 2.14×10^{-5} to 5.38×10^{-5} m as time changes from $t = 0$ to $t = 0.67$ s. At $x = 4$ mm, the radius of curvature increases linearly from 1.41×10^{-4} to 2.49×10^{-4} m as time changes from $t = 0$ to $t = 0.33$ s. The gradient of the radius of curvature for the growing drop at $x = 4$ mm is more than 6 times larger than that at $x = 3$ mm. Figure 9 shows a comparison of the apparent contact angles of the growing drop at different locations. For both cases, the apparent contact angle is not a function of time. The apparent contact angles of the drops at $x = 4$ mm are about 5.9°, half as much as those of the drops at $x = 3$ mm in Figure 3 (about 13°). We find that the drop with the smaller contact line velocity has a larger apparent contact angle. We believe that this unexpected result is due to the additional effect of the liquid−vapor interfacial temperature difference and, therefore, thin film adsorption, which will be discussed next.

The temperature difference between vapor and quartz wall (ΔT_{vw}) for the dropwise condensation can be measured directly. Compared with the vapor cross-sectional area ($\sim 3 \times 3$ mm), the average length scale in the liquid is much smaller, in the magnitude of a micron. Since the vapor flow encounters minimum resistance, the pressure level in the vapor is approximately uniform, and the vapor temperature is obtained from the saturated vapor pressure measured by a pressure transducer. We found that the pressure measurements correlated with the inside wall temperature in the region of condensation. The wall temperature is measured using a thermocouple on the outside quartz wall. ΔT_{vw} consists of the extremely small liquid−vapor interfacial temperature difference (ΔT_{lvv}) and the temperature difference between the liquid−vapor interface temperature and the wall temperature. Even though the extremely small interfacial temperature difference (ΔT_{lvv}) for the growing drop cannot be measured directly, it can be obtained from eq 13. It is a function of time, radius of curvature, and apparent contact angle. Figure 10 shows a comparison of the absolute value of the interfacial temperature difference for the growing drop at different locations. We find that the drop with the larger contact angle (and larger $|K|$) has the larger interfacial temperature difference.

In eq 10, the interfacial heat flux is proportional to the rate of change of the radius of curvature of the growing drop. Experimental results show that the radii of curvature for the growing drop increase linearly with time, and the rate of change of the radius of curvature for the growing drop at $x = 4$ mm ($\theta_d = 5.9°$) is more than 6 times larger than that at $x = 3$ mm ($\theta_d = 13°$). Thus, using eq 10, the interfacial heat flux at $x = 4$ mm ($q''_{lv} = -1701$ W/m^2) is

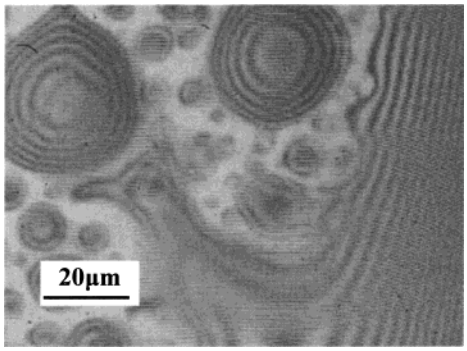

Figure 11. Drop at $x = 4$ mm in the same CVB (i.e., the same value of the P_v) as that in Figure 3.

larger than that at $x = 3$ mm ($q''_{lv} = -1229$ W/m^2). According to the Kelvin−Clapeyron model, eq 2, condensation is promoted by subcooling ($\Delta T < 0$) and hindered by high liquid film pressure ($\Delta P = (P_l - P_v) > 0$). For comparison, eq 2 is rewritten using the numerical values of the coefficients as eqs 14 and 15.

$$q''_{lv} = 3.66 \times 10^6(T_{lv} - T_v) + 1.753(P_l - P_v) \qquad x = 3 \text{ mm} \quad (14)$$

$$q''_{lv} = 8.48 \times 10^6(T_{lv} - T_v) + 4.632(P_l - P_v) \qquad x = 4 \text{ mm} \quad (15)$$

Although the interfacial temperature difference (subcooling) is larger at $x = 3$ mm than that at $x = 4$ mm, the radius of curvature at $x = 3$ mm is much smaller, and the hindering effect of the pressure jump on condensation is larger at $x = 3$ mm. Although the above comparison was made using results for different pressure levels, the drops at the same pressure level but different axial locations showed similar trends;[67] see Figure 11. These results demonstrate that the use of the CVB technique for obtaining data leads to an enhanced understanding of condensation and, therefore, the contact line motion.

In general, we find, from our experiments, that drops with larger radii of curvature have smaller pressure jumps at the liquid−vapor interface which lead to smaller interfacial temperature differences and thicker ultrathin films between the drops. Although the film thicknesses between the drops were not measured, they could be qualitatively observed. These thicker ultrathin films should also lead to smaller contact angles. However, these near-equilibrium advancing contact angles were found to be larger than the equilibrium value independently measured for the corner meniscus, $\theta_e = 4.9°$ at $T_v = 23$ °C. These results demonstrate the macroscopically observed coupling between the interfacial shape, interfacial mass flux, interfacial temperature difference, and the spreading velocity. Both of the spreading condensing drops discussed above have a contact angle larger than equilibrium which is commonly observed in isothermal spreading[1−27] and predicted for nonisothermal spreading.[28−30,49] The condensed adsorbed thin film has a significant effect on the spreading.

For equilibrium systems, Sharma[69] presented eq 16 for the apparent contact angle as a function of the excess free energy per unit area.

$$\sigma_l(\cos\theta - 1) = \Delta G(h_e) \quad (16)$$

in which h_e is the thickness of the adsorbed ultrathin flat film adjacent to the sessile drop. In eq 17, the excess free energy is given in terms of the apolar, S^{LW}, and polar, S^P, components of the spreading coefficient.

$$\Delta G(h_e) = S^{LW}\left(\frac{d_0^2}{h_e^2}\right) + S^P \exp\left[\frac{d_0 - h_e}{l_0}\right] \quad (17)$$

in which d_0 is an equilibrium cutoff distance and l_0 is a correlation length for polar interactions. In our case, $S^{LW} > 0$, $S^P < 0$, and $\Delta G(h_e) < 0$. Using techniques suggested by Sharma,[70] we found[71] $S^{LW} = 5.436$ mJ/m^2 and $S^P = -5.517$ mJ/m^2. In essence, using a measured equilibrium contact angle of $\theta = 2.73°$ for apolar tetradecane with a surface tension of $\sigma_l = 26.13$ mJ/m^2, the apolar component of the surface tension of the substrate was found to be equal to $\sigma_s^{LW} = 26.10$ mJ/m^2 . Using this value and the apolar component of the surface tension of ethanol ($\sigma_{lv}^{LW} = 20.30$ mJ/m^2), the apolar component of the spreading coefficient for the ethanol/quartz system, S^{LW}, was obtained. Using S^{LW}, the total surface tension of ethanol, $\sigma_l = 22.20$ mJ/m^2, and a measured equilibrium contact angle of $\theta = 4.9°$, S^P was obtained for the ethanol/quartz system. The minimum value of ΔG occurs at equilibrium, and the value of ΔG increases ($\Delta G \rightarrow 0$) with an increase in adsorbed film thickness. An increase in the film thickness would also cause flow. Using these equilibrium models for our near-equilibrium data indicates that our decrease in contact angle is a measure of the change in film thickness due to the combined effects of ΔT and ΔP. For the complex process described above, the ultrathin film thickness at $x = 4$ mm is larger than that at $x = 3$ mm. This larger film thickness would also have a lower viscous resistance to flow. However, in all these very small systems, inertial effects would be minimal.

Conclusions

1. A unique experimental design and the image-analyzing technique were used to study the growth characteristics of sessile drops.

2. Using interference microscopy measurements of the transient liquid film profile to obtain the pressure field and a Kelvin−Clapeyron model of interfacial mass flux, the interfacial temperature difference was obtained.

3. At constant heat flux, while the radius of curvature of the growing drop increased linearly with time, the apparent contact angle remained the same during growth.

4. The contact angle, the interfacial subcooling, the interfacial pressure jump, the spreading velocity, interfacial mass flux, and adsorption are coupled at the moving contact line.

5. Motion and the apparent contact angle are governed by the condensed adsorbed thin film thickness and curvature at the contact line.

Acknowledgment. This material is based on work supported by the National Aeronautics and Space Administration under Grant No. NAG3-2383. Any opinions, findings, and conclusions or recommendations expressed in this publication are those of the authors and do not necessarily reflect the view of NASA.

LA020040B

(69) Sharma, A. *Langmuir* **1998**, *14*, 4915.

(70) Sharma, A. *Langmuir* **1993**, *9*, 861.

(71) Gokhale, S. J. Personal communication.